Structural, Morphological and Dielectric Spectroscopy Analysis of Double Perovskite Bi_2MnNiO_6 Electronic Material

A. Tripathy[a], S. N. Das[a], *, S. Bhuyan[a], and R. N. P. Choudhary[a]

[a]*Department of Electronics and Communication Engineering, Siksha 'O' Anusandhan (Deemed to be University), Bhubaneswar, 751030 India*

*e-mail: satyaprakashdas@soa.ac.in

Abstract —Exploring as well as examining novel functional double perovskite material represents an important aspect in the field of electronic devices. In this present study the electronic material Bi_2MnNiO_6 has been framed through high temperature solid state ceramic processing method. Its electronic structure, morphological and electrical characteristics has been evaluated. Its structure is found to be monoclinic through XRD analysis. The uniform and compact grain distribution has been observed form the micrographs. The impedance analysis of the ceramic suggests negative temperature coefficient of resistance behaviour. The important electrical properties associated with this compound may be essential in the development of next generation electronic devices.

1. INTRODUCTION

The perovskites are one of the excellent and intriguing classes of material which have a wide variety of application in the field of next generation nanoelectronics, optoelectronics, solar cells, fuel cells, super capacitors, memories, sensors, tunable microwave devices, piezoelectric devices, etc. [1−6]. These can be of various types such as general perovskite—ABO_3 (ex: $BiFeO_3$, $BaTiO_3$, $CaTiO_3$), layered perovskite—A_2BO_4 (ex: K_2NiF_4, Sr_2RuO_4,), double perovskite—$A_2BB'O_6$ (ex: Ba_2TiRuO_6) and triple perovskite—$A_2A'B_2B'O_9$ (ex: $La_2SrCo_2FeO_9$), etc. [7−13]. Because of its interesting characteristics like ionic conduction, superconductivity, metal-insulator transition, excellent dielectric, magnetic and ferroelectric properties, till now this is in the lime light for the researchers and this research field proliferates day by day. Among the various perovskites, double perovskites are one of the exceptional structures in solid-state physics, and it can accommodate most of the metal ions in the periodic table at B and B'-site with different anions at A-site. Proper selection and incorporation of various metal ions along with the alkali, alkaline earth or rare earth ions can permit to apprehend a large diversity of physical and chemical properties in DPs [14−16].

Considering DPs prominence, the multiferroic materials having both ferroelectric and ferromagnetic orderings based novel double perovskite electronic material Bi_2MnNiO_6 has been formulated and fabricated by using solid state reaction route. In this studied material Bi^{+3} ions are positioned at A-site and magnetic elements Ni^{+2} and Mn^{+4} ions are well-ordered at the B and B' site. An attempt has been made to provide its structural, morphological, dielectric as well as electrical characteristics which can be use full for development of electronic device and sensor.

2. EXPERIMENTAL PROCESS

The chosen double perovskite ceramic sample of Bi_2MnNiO_6 is fabricated by usual solid state reaction path. It starts through the raw material selection as the first step. Depending upon the expected nature of the desired sample and reaction conditions the reactant chemicals are chosen. Here mostly the oxides (Bi_2O_3, MnO_2, and NiO) of high purity (>99.9%) are used which are obtained from Loba Chemicals Pvt. Ltd. These raw oxides are dried carefully, and then weighed according to their required mass percentage. To enhance the rate of reaction the raw materials are fine grained and mixed cautiously by dry grinding from beginning to end with mortar and pestle for nearly 2 hours to get a homogeneous solution of these raw oxides. It is followed by wet grinding by mixing the homogenous dry mixture with methanol (an organic volatile liquid), in order to ensure the homogeneity of the mixture. The wet grinding process continued till all the entire liquid gets evaporated, leaving residual homogeneous mixture. The evaporation process usually takes nearly 1 hour to be complete. Then this pow-
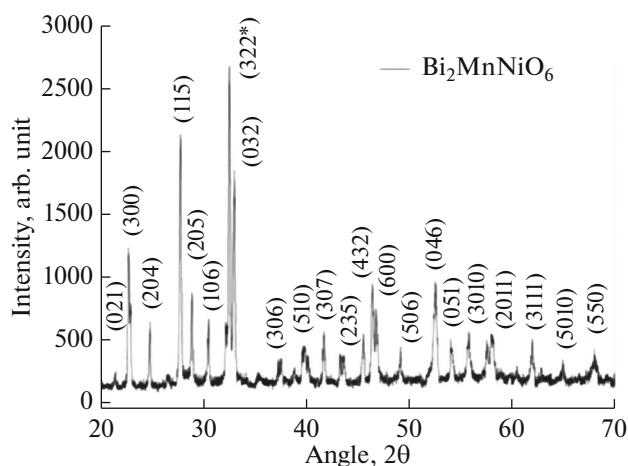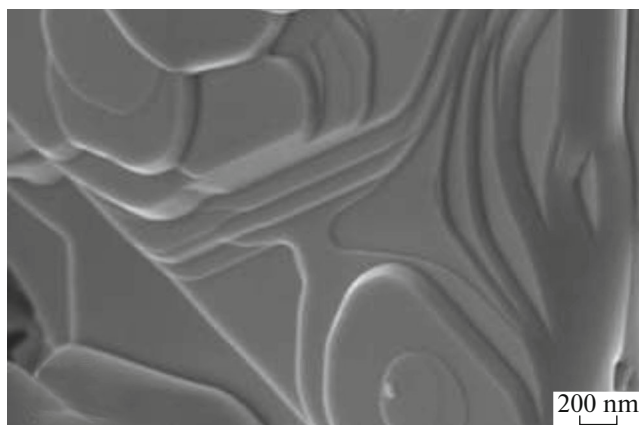
Fig. 1. Room tempertaure XRD pattern of Bi_2MnNiO_6.

Fig. 2. SEM micrograph of Bi_2MnNiO_6.

der raw sample is calcined at an optimized temperature (750°C) through a high temperature furnace for an extent of 4 hours. For the calcinations process the mixture is kept in an alumina crucible, because it can sustain very high temperatures, even much higher than the melting temperature of the chosen double perovskite. Next step in the process of fabrication includes the grinding of the reduced calcined powder (with little lump formation) into fine powder form, so that XRD can be performed smoothly. From the XRD analysis the formation of desired compound can be confirmed. Now circular pellets (disks) are formed with the help of hydraulic press. PVA is added as binder with the calcined mix to provide the binding to the powder. Then the disk shaped pellets are set for sintering process at a high temperature of nearly 800°C. Then the microstructures of sintered disk pellets are investigated with Scanning Electron Microscopy. Then silver paste is applied to the both surfaces (i.e. bottom as well as top) of the polished pellets which act as the electrodes of a parallel plate capacitor.

The temperature dependent dielectric parameters are studied by using N4L PSM1735: phase sensitive meter. The related dielectric components and the impedances are considered for temperature ranges from 25 to 250°C with frequency: 1 kHz–1 MHz.

## 3. RESULTS AND INVESTIGATIONS

a. Structural and Morphological Properties

Figure 1 shows the X-ray diffraction structure of the prepared compound Bi_2MnNiO_6. The obtained sharp peaks of the XRD analysis are indexed by means of a computer program (POWD) [17]. For the newly formed compound, the Miller Index values (*hkl*) are nearly equal to the structural parameters of the material. The best fitting of the structure formed was found to be monoclinic with parameters as $a = 7.28$ Å, $b = 5.05$ Å, $c = 5.23$ Å and $\beta = 99.70°$ along with a standard deviation (SD) = 0.0053. The projecting peaks show a new perovskite structure which is different from the parent elements. Thus, the formation of a new polycrystalline compound is confirmed [18].

The Fig. 2 depicts the microstructure of Bi_2MnNiO_6. The microstructure signifies that the grains are looking like compact melted slabs that are stacked one over other. This compact nature enables proper electrical measurements of the pallet samples.

b. Dielectric Analysis

By measuring the real and imaginary parts of impedance, permittivity and electric modulus of the double perovskite material Bi_2MnNiO_6, some data can be obtained which are in acquaintance with the micro structural properties. Impedance spectroscopy is an influential approach to disassociate the contribution of grain and grain boundaries effect to the total conductivity or resistivity of the compound. This method also permits to estimate and separate the contribution in frequency domain to the overall electrical properties due to electrode reactions at the electrode/material interface. The properties of the compound dependent on frequency has been illustrated using different parameters that are related to one another such as permittivity, dielectric loss, complex impedance, conductivity and electric modulus.

At certain selected frequencies, the temperatures dependent relative dielectric constant (ε_r) as well as the tangent loss (tan δ) of electronic compound Bi_2MnNiO_6 is depicted in Fig. 3. The dielectric constant is increasing with gradual increase in temperature and attends maxima. This maxima or peak simultaneously depends upon the temperature and frequency. After attaining the maxima, the relative permittivity decreases with further progression of temperature. Typical relaxor characteristic like shifting of peak and peak broadening has been observed in this material. At higher frequency the peaks become more
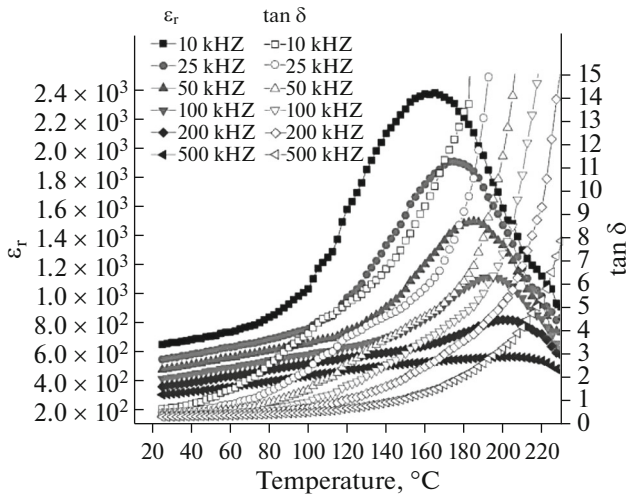
Fig. 3. Temperature dependence of dielectric constant and tangent loss at selected frequencies of Bi_2MnNiO_6.

Fig. 4. Frequency dependence of dielectric constant and tangent loss at selected temperatures of Bi_2MnNiO_6.

flat and the peak shifts towards higher temperature. These characteristics confirm the relaxor nature of this material [19, 20]. Similarly, the tangent loss also increases with the rise in temperature. The Fig. 3 also depicts that the tangent loss is becoming constant at higher frequencies as compared to the lower frequencies with an increase in temperature. It is also observed that at higher frequency regions, the dielectric constant and tangent loss both decreases. So, it can be concluded that the newly formed ceramic material exhibits broad behavior of dielectric features.

Figure 4 illustrates the relative dielectric constant (ε_r) and tangent loss (tan δ) wrt frequency at selected temperatures for Bi_2MnNiO_6. It can be observed that both the dielectric constant as well as tangent loss decreases progressively with an increase in the frequency. The growth rate of tan δ is sluggish at lower temperature regions, but at higher temperature regions the losses are reasonably sharp. This phenomenon is observed because of the presence of thermally active charge carriers and defects like oxygen vacancy. At higher range of temperature vacancies (oxygen vacancy, lattice vacancies) and defects (such as thermally activated charge defect, electronic/ionic defect, boundaries, dislocation, etc.) cause the relaxation process while at lower-temperature zone immobile charges causes the same effect [21, 22]. As the temperature increases and transport of thermally activated space charges takes place, there is an improvement of relative dielectric constant in the material. The volatile nature of Bismuth during heating process (which includes both calcinations and sintering methods) contributes to the oxygen vacancy of space charges [23]. The dielectric peaks move towards high temperature zone as the frequency increases. It may happen due to the presence of magnetoelectric influence in all solid state materials. The peaks confirm the change of electrical dipole
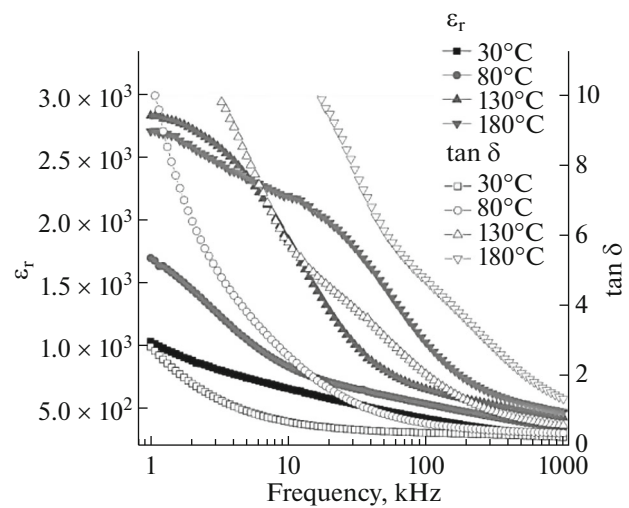
from one state to another because of the switch in electromagnetic state [24].

c. D.C. Conductivity Analysis

The DC conductivity ($I \sim V$) analysis is given in Fig. 5 at few selected temperature values (25 to 150°C). From the graph we can find the relationship between the voltage and current. It is observed that at room temperature it shows non-ohmic (nonlinear) like behavior. This nonlinear behavior may be due to the semiconducting nature of the materials [25]. Again after a definite value of voltage, the current reaches a highest value, and then saturates. With the rise in temperature the semiconductor behavior gradually vanishes and its property becomes linear.
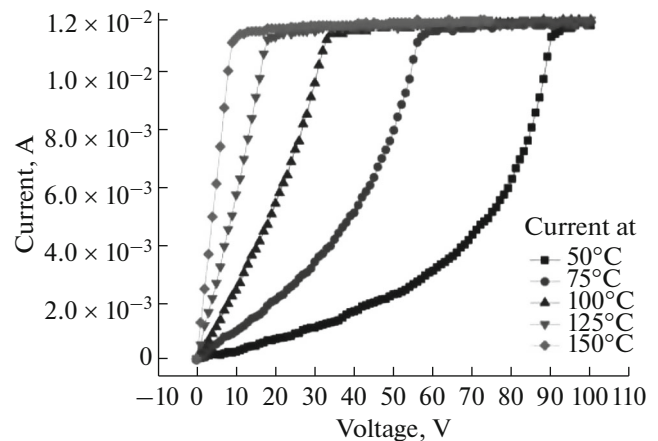
Fig. 5. $I-V$ characteristics of Bi_2MnNiO_6.
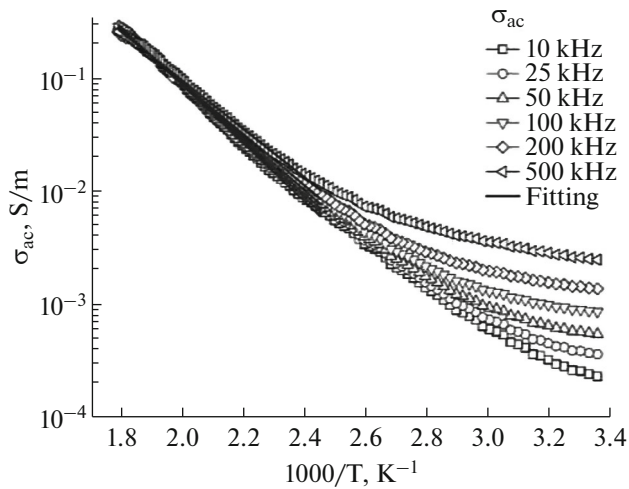
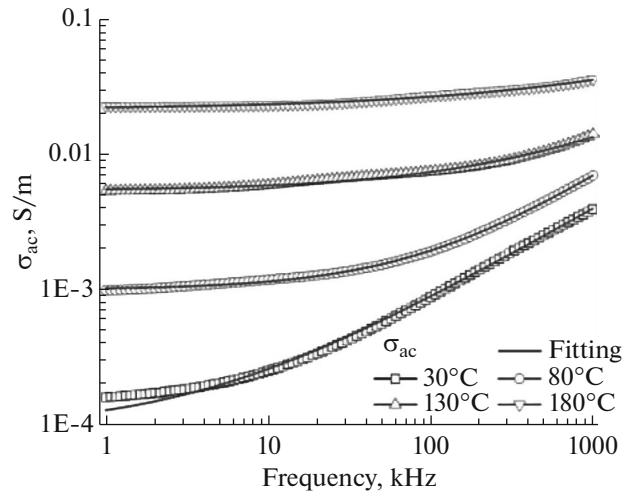**Fig. 6.** Temperature dependent ac conductivity spectrum at selected frequency of Bi_2MnNiO_6.

Fig. 7. Frequency dependent ac conductivity spectrum at selected temperature of Bi_2MnNiO_6.

d. A.C. Conductivity Investigation

Figure 6 depicts the temperature characteristics of the ac conductivity $[\sigma_{ac}(\omega)]$ of Bi_2MnNiO_6 double perovskite with various frequencies. Also the frequency dependent ac conductivity characteristics at some selected temperature values are shown in Fig. 7. The ac conductivity depends on the dielectric values of the material, and can be calculated with the help of the following equation: $\sigma_{ac} = \omega \varepsilon \varepsilon_0 \tan \delta$. The activation energy (E_a) of the ceramic can be considered with the help of the equation: $\sigma_{ac} = \sigma_0 \exp(-E_a/kT)$ where σ_0 represents the pre-exponential factor and k represents the Boltzmann constant [26, 27]. Occurrence of multiple slopes at different frequencies and temperature range signifies the presence of more than one conduction processes [28]. The activation energy values are listed in Table 1. From the table it is concluded that the activation energy decreases with rise of frequency. A uniform response of conductivity is observed at low frequency region whereas at higher frequency its value increases. The conductivity characteristic can be explained with the help of [29]. The Jonscher's power law is expressed as $\sigma_{ac} = \sigma_{dc} + A\omega^n$, where σ_{dc} is dc conductivity, A is the temperature dependent constant and n is temperature dependent exponent ($0 \le n \le 1$). Here the strength of polarization and the degree of interaction between movable ions in the lattices are determined from A and n respectively. The obtained values of A and n values are depicted in Table 2. From the values of A and n it can be noticed that with the rise in temperature the A value increases whereas the value of n decreases. The origin of ac conductivity in the relaxation phenomenon may arise due to movable charge carriers, which are generally present inside every ceramic material. It can also be said that frequency independent smooth region for lower frequency values results from the dc conductivity property and the dispersion at the higher frequencies results from the ac conductivity property of the studied compound.

Table 1. Activation energy at different frequencies of the compound Bi_2MnNiO_6

	Activation energy of Bi_2MnNiO_6 at the temperature range 130 to 200 °C	
1	1 kHz	0.47 eV
2	10 kHz	0.44 eV
3	100 kHz	0.41 eV
4	1 MHz	0.31 eV

e. Impedance Spectrum Analysis

The impedance spectrum of Bi_2MnNiO_6 is depicted in Fig. 8 which consists of the real part Z' and the imaginary part Z'', at different temperatures. The dielectric characteristics of the ceramic in terms of frequency are measured with the Impedance Spectroscopy method. The measurement is done on the basis of interaction of the electric field and the electric dipole moment. From this the frequency response, energy stored and the dissipation properties of the compounds can be calculated. Impedance Spectroscopy (IS) is generally used to explore the electrical

activities and the conduction properties of the ceramics. It can be observed that as the frequency as well as temperature increases, Z' values decreases. This establishes the NTCR nature of the ceramic material. The frequency dependent dielectric properties are described with the complex parameters. They are merged together at the elevated frequency region in spite of temperature variations, which happens because of the release of space charge inside the ceramic material.

The Nyquist plot i.e. complex impedance spectrum at few chosen temperatures with frequency range from of 1 kHz to 1MHz of Bi_2MnNiO_6 is depicted in Fig. 9 which represents the relationship of microstructure with electrical properties. This plot can be interpreted by using the mathematical formula as:

$$\frac{\varepsilon_r^* - \varepsilon_{r\infty}'}{\varepsilon_{rs}^* - \varepsilon_{r\infty}''} = \frac{1}{(1 + j\omega t)^{1-\alpha}}.$$

The above expression can be simplified as the traced semicircle equation as follows:

$$\left(\varepsilon_r'(\omega) - \frac{1}{2}(\varepsilon_{rs}' - \varepsilon_{r\infty}')\right) + \varepsilon_r''(\omega)^2 = \frac{1}{4}(\varepsilon_{rs}' - \varepsilon_{r\infty}')^2.$$

Where the parameter α describes the distribution of relaxation time in the material, $\varepsilon_{r\infty}'$ and ε_{rs}' are the intercept of the semicircle on x-axis represents high and low frequency dielectric constant. From the graph it is observed that, with the advancement of temperature the semicircle arcs or curves bend towards the origin forming a semicircular arc with a displacement of the center. Hence a semicircle arc can be outlined to characterize the increase in conductivity of the sample with the elevation of temperature [20]. The effect of grain and grain boundaries can be interpreted from this semicircular nature of the plot. It mainly utilities
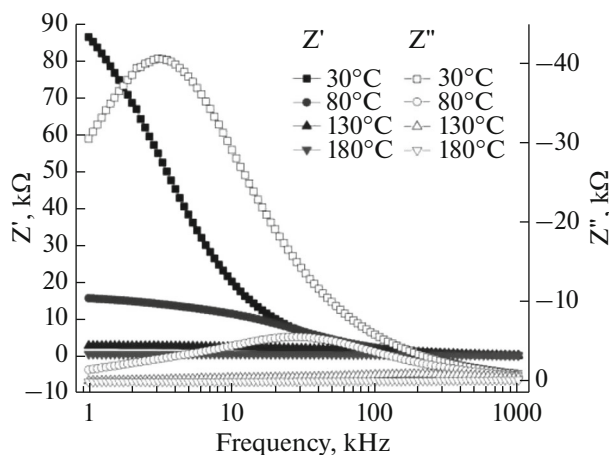
Table 2. The values of σ_{dc}, A and n at different temperatures of the compound Bi_2MnNiO_6

Temperature, °C	σ_{dc}	A	n
30	9.64×10^{-4}	3.06×10^{-7}	0.68
80	1×10^{-3}	9.47×10^{-8}	0.80
140	5×10^{-3}	1.94×10^{-6}	0.60
200	2×10^{-2}	3.45×10^{-5}	0.43

the bulk material (grain interior) and consequently they might be interpreted as different parameter of an electrical circuit which is shown in the Fig. 10 which is obtained by using Z-win software. The values different circuit parameters obtained from the fitting model such as $R_b(\Omega)$, $C_b(F)$, CPE (Constant Phase Element), $R_{gb}(\Omega)$ and C_{gb} are shown in Table 3. This technique is very much helpful to identify and correlate the observed relaxation phenomenon with the atomic as well as micro structural attribute (both grain and grain boundary effect) of the material. The existence of certain depressed semicircle arc r in Nyquist plot with center towards real axis represents the presence of non-Debye type relaxation with dissemination relaxation time [22] in all the synthesized compounds.

f. Complex Electric Modulus Analysis

The frequency variation modulus spectrum i.e M' and M'' at various temperatures of the prepared ceramic is shown in Fig. 11. M' modulus factor is almost nil in small frequency regions and extend
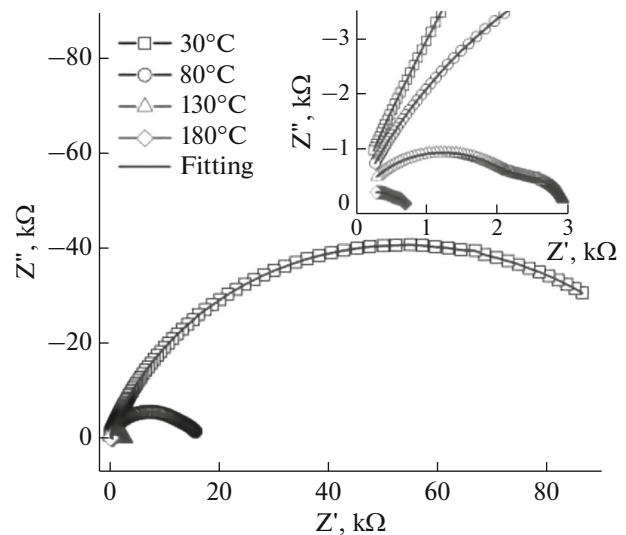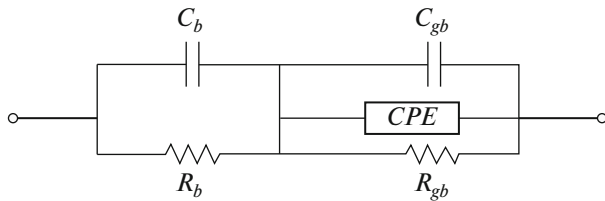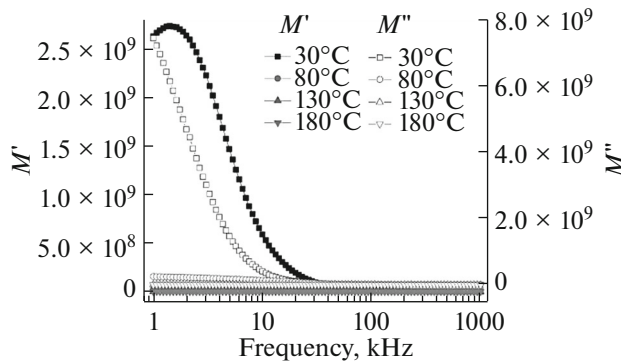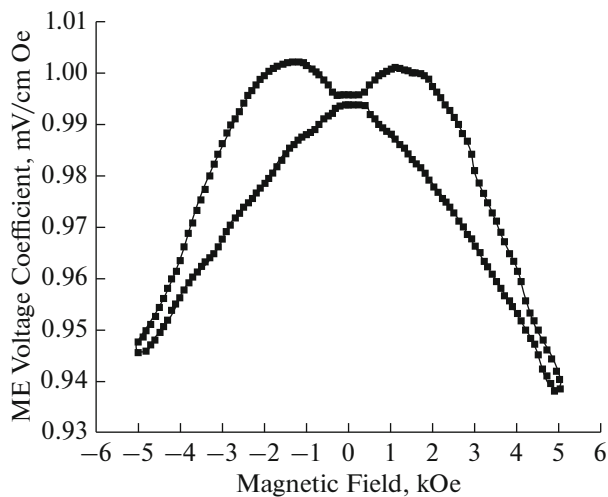

Fig. 8. Frequency dependence complex impedance properties at selected temperatures of Bi_2MnNiO_6.

Fig. 9. Nyquist plot of Bi_2MnNiO_6 at selected temperature.

Fig. 10. Equivalent electrical circuit model for Nyquist plot.

monotonically with frequency and then overlap in the upper frequency regions. The conduction method and movement of short range charge carriers within the fabricated material contributes to this type of result. We can observe that the M'' modulus factor crest moves to prominent frequency side. The lengthening of relaxation peak at different selected temperatures indicates non- Debye relaxation mechanism in the synthesized compounds [29, 30].

Fig. 11. Frequency dependence complex modulus properties at selected temperatures of Bi_2MnNiO_6.

g. Magneto-Electric Coupling Coefficient (ME)

The *ME* coefficients (Magneto Electric Coupling Coefficient) of Bi_2MnNiO_6 have been studied by simultaneous application of both ac and dc magnetic fields. The *ME* voltage coefficient α_{ME} i.e. magneto-electric coupling parameter is defined as follows [27]:

$$\alpha_{ME} = \frac{dE}{dH} = \frac{1}{d}\frac{dV}{dH} = \frac{V_{out}}{h_0 d} \qquad (iv)$$

From the above equation we can see that *ME* voltage coefficients depends on the change in electric field (E) with respect to the applied magnetic field (H). Here 'V' is the developed *ME* voltage across the sample, 'd' is the thickness of the sample and h_0 is the magnitude of the ac magnetic field. The effect of dc applied magnetic field on *ME* voltage coefficient is shown in Fig. 12.

4. CONCLUSIONS

The electronic materials Bi_2MnNiO_6 has been synthesized using the basic solid state reaction method. The obtained experimental results corroborate the effect of Nickel substitution in the morphological behavior with reduced grain size, monoclinic crystal structure, enrichment in capacitive behavior, negative temperature coefficient of resistance, reduced residual polarization and raise in frequency dependent ac conductivity along with non-Debye type of conductivity relaxation. The structural, morphological, dielectric constant, loss tangent, impedance characteristics, structure-property relationship, resistive, conductive as well as capacitive characteristics substantiate the prepared materials as an emerging candidate for different electronic applications.

Fig. 12. Variation of magneto-electric coefficient of Bi_2MnNiO_6.

Table 3. Fitting parameters of grain and grain boundary resistance as well as capacitance of impedance parameters of the compound Bi_2MnNiO_6

T, °C	$R_b(\Omega)$	$C_b(F)$	CPE	$R_{gb}(\Omega)$	C_{gb}
30	4.304E+06	2.327E-09	4.227E-09	2.805E+03	3.101E-07
80	3.001E+03	1.134E-09	7.401E-09	8.206E+05	4.062E-07
140	1.234E+02	6.342E-08	1.502E-08	6.318E+04	2.263E-07
200	4.520E+01	5.374E-07	4.125E-08	2.503E+04	2.452E-07

REFERENCES

1. W. Eerenstein, N. D. Mathur and J. F. Scott, Nature **442**(7104), 759 (2006).

2. Y. Lan, X. Feng, X. Zhang, Y. Shen and D. Wang, Phys. Lett. A **380**(37), 2962 (2016).

3. A. K. Paul, M. Reehuis, V. Ksenofontov, B. Yan, A. Hoser, D. M. Tobbens, P. M. Abdala, P. Adler, M. Jansen and C. Felser, Phys. Rev. Lett. **111** (16), 1 (2013).

4. M. Green, A. H. Baillie and H. J. Snaith, Nat. Photonics **8** (7), 506 (2014).

5. G. Volonakis, M. R. Filip, A. A. Haghighirad, et al, J. Phys. Chem. Lett. **7** (7), 1254 (2016).

6. S. N. Das, S. K Pradhan, D. P. Kar, S. Bhuyan and R. N. P. Choudhary, J Mater. Sci. Mater. Electron. **29** (11), 9375 (2018).

7. G. Blasse, J. Phys. Chem. Solids **26** (12), 1969 (1965).

8. C. L. Bull, D. Gleeson and K. S. Knight, J. Phys.: Condens. Matter **15** (29), 4927 (2003).

9. R. I. Dass and J. B. Goodenough, Phys. Rev. B **67**, 014401 (2003).

10. A. I. Kurbakov and G. V. Sarapin, J. Surf. Invest.: X-ray, Synchrotron Neutron Tech. **9** (3), 530 (2015).

11. M. T. Anderson, K. B. Greenwood, G. A. Taylor and K. R. Poeppelmeier, Prog. Solid State Chem. **22**(3), 197 (1993).

12. S. Afroze, A. Karim, Q. Cheok, S. Eriksson, and A. K. Azad, Front. Energy, **13** (4) 770 (2019).

13. A. K. Tomar, A. Joshi, S. Atri, G. Singh, and R. K. Sharma, ACS Appl. Mater. Interfaces, **12** (13), 15128 (2020).

14. P. G. Radaelli, D. E. Cox, M. Marezio, S. W. Cheong, P. E. Schiffer and A. P. Ramirez, Phys. Rev. Lett. **75**, 4488 (1995).

15. H. J. Feng and F. M. Liu, Phys. Lett. A **372** (11), 1904 (2008).

16. Y. Q. Lin and X. M. Chen, J. Am. Ceram. Soc. **94** (3), 782 (2010).

17. E. Wu, J. Appl. Crystallogr. **2.2** (5), 506 (1989).

18. K. Singh, S. A. Band and W. K. Kinge, J. Ferroelectr. **306** (1), 179 (2004).

19. E. Nyamdavaa, E. Uyanga, G. Sevjidsuren and P. Altantsog, J. Surf. Invest.: X-ray, Synchrotron Neutron Tech. **11** (2), 336 (2017).

20. S. N. Das, S Pradhan, S. Bhuyan, R. N. P. Choudhary and P. Das, J. Electron. Mater. **46** (3), 1637 (2017).

21. K. K. Mishra, A. T. Satya, A. Bharathi, V. Sivasubramanian, V. R. K. Murthy and A. K. Arora, J. Appl. Phys. **110** (12), 123529 (2011).

22. S. N. Das, A. Pattanaik, S. Kadambini, et al., J Mater. Sci. Mater. Electron. **27** (10), 10099 (2016).

23. J. E. Garcia, V. Gomis, R. Perez, A. Albareda and J. A. Eiras, Appl. Phys. Lett. **91** (4), 042902 (2007).

24. K. S. Kumar, C. Venkateswar and D. Kannan, J. Phys. D: Appl. Phys. **45** (41), 415302 (2012).

25. A. Tripathy, S. N. Das, S. K. Pradhan, S. Bhuyan and R. N. P. Choudhary, J Mater. Sci. Mater. Electron. **29**(6), 4770 (2018).

26. H. Jain and C. H Hsieh, J. Non-Cryst. Solids **174**, 1408 (1994).

27. D. P. Almond and A. R. West, Solid State Ionics **11** (1), 57 (1983).

28. S. K. Pradhan, S. N. Das, S. Bhuyan, C. Behera and R. N. P. Choudhary, J Mater. Sci. Mater. Electron. **28**(2), 1186(2017).

29. Y. Zhang, J. P. Zhou, Q. Liu, S. Zhang and C. Y. Deng, Ceram. Int. **40** (4), 5853 (2014).

30. S. Halder, S. Bhuyan, S. N. Das, S. Sahoo, R. N. P Choudhary, P. Das and K. Parida, Appl. Phys. A: Mater. Sci. Process. **123**(12), 781 (2017).